-Please check throughout the text for spelling errors, figures, and tables.
-Please check title, author names, affiliations and emails.
-Please check keywords and codes.

Journal of Computational Biophysics and Chemistry

Research

Cite This: *J. Comput. Biophys. Chem.* **2022**, *21* ~~(3)~~, 1–12

Development of Pyrazole Harbouring Novel Leads Against β-Amyloid Protein Fibrillation by *in silico* Drug Design

AQ: Approved

Puja Mishra*, Sujata Biswas*, Sudipta Baur*, Souvik Basak*,‡, Arup Mukherjee†,‡ and Anindya Basu +

+School of Pharmaceutical Sciences, Rajiv Gandhi Proudyogiki Vishwavidyalaya, Bhopal, India

AQ: Souvik Basak is the only corresponding author

AQ: Provided

*Dr. B. C. Roy College of Pharmacy & Allied Health Sciences, Durgapur, WB, India
†Department of Biotechnology, Maulana Abul Kalam Azad University of Technology, WB, India
‡Corresponding authors. E-mail: *souvik_basak1@yahoo.com, souvikb9@gmail.com*

ABSTRACT: Amyloid β (Aβ) peptide monomers polymerize to form insoluble amyloid fibril aggregates and accumulate as senile plaques which eventually leads to cognitive impairment. Modulating abnormal amyloid aggregation can be considered a therapeutic target for Alzheimer's disease. Recent studies support that Curcumin interferes with larger protein aggregate formation by destabilizing the salt bridge (Asp 23-Lys 28) of Aβ protein. The chemical library of curcumin derivative with pyrazole, isoxazole, and isothiazole showed considerable binding affinity comparable to that of curcumin. *In silico* docking studies of the library of the compound, revealed strong binding affinity with Aβ protein and β-secretase enzyme (BACE1). *De novo* ligand design coupled with manual pharmacophore mapping of our best-fitting lead revealed another ligand having a potential binding affinity with both Aβ protein and BACE-1. Both the compounds passed Lipinski's Rule of Five, *in silico* toxicity testing by admetSAR, and pharmacophore overlaps with Verubecestat, a compound under clinical trial against Alzheimer's disease. MD dynamic simulation study revealed the stability of protein after it binds to our ligand. Secondary structure determination was also done to observe the changes in α and β sheets of the protein with and without ligand binding. Ligand-based drug design was also carried out via pharmacophore mapping and searching the molecules via zinc database.

KEYWORDS: Amyloid-β; fibril destabilization; pyrazole; *de novo* ligand design; molecular docking; MD simulation; pharmacophore mapping.

1. INTRODUCTION

Curcumin is a bioactive diarylheptanoid obtained from *Curcuma longa* rhizome. Curcumin (1, 7-bis-(4-hydroxy-3-methoxyphenyl)-1,6-heptadiene-3,5-dione) contains two methoxy phenol groups separated by a seven carbon linker and α–β unsaturated β-diketone groups. The α–β unsaturated β-diketone exists in keto-enol tautomeric form of which enol form is a more stable and dominant type. The aromatic ring is involved in π–π interaction and hydroxyl group and keto-enol group is involved in hydrogen bonding.[1] The seven carbon linkers may adopt a conformer that is essential for lipophilic interaction. Curcumin binds to many proteins and changes their conformation and stability of protein molecules thus inhibiting aggregation.[2] Curcumin may be involved in metal chelation, inhibition of Amyloid-β (Aβ) 42 protein fibrillation and may trigger anti-oxidative properties due to the presence keto-enol moiety in its structure.[3–8]

Amyloid-β fibril formation is regarded as the etiology of Alzheimer's disease. Amyloid-β is a protein formed after sequential cleavage of the amyloid precursor protein (APP), a transmembrane glycoprotein that can be cleaved by the proteolytic enzymes α-, β- and γ-secretase.[9] APP undergoes a nonamyloidogenic pathway when it is cleaved by α and γ-secretase sequentially and forms APP Intracellular domain (AICD) and soluble APPα. However, successive cleavage of APP by β and γ secretase enzymes forms soluble APPα along with an insoluble Amyloid-β protein.[10] Amyloid-β is a protein having 36–42 amino acids that form amyloid plaques in the brain of Alzheimer's patients. They predominantly exist in two isoforms, Aβ-40 and Aβ-42, Aβ-42 being the major amyloidogenic forms of

Received: 6 January 2022
Accepted: 4 March 2022
Published:

DOI: 10.1142/S2737416522500193
J. Comput. Biophys. Chem. **2022**

the peptide. The peptide bears 16 hydrophilic residues (Asp 1-Lys 16) and the rest of the peptide (Leu 17-Val-40) is hydrophobic. An earlier report has elicited that within this peptide, the amino acid residues forming KLVFFAE fragment (Lys 16-Glu 22) form the core for fibril formation After this nucleation, oligomers extend to form larger aggregates in the salt bridge region (Glu 22-Gly 29). Aβ-42 dimer gets stabilized by the salt bridge and HHQK fragment site contains His-13, His 14 residues which bring a conformational change of Aβ from α-helix to β-sheet structure.[11,12]

Curcumin modulates protein fibril aggregation by binding to monomeric species of fibrillation pathway and tailors the intermolecular interactions between the polypeptides. Functional groups of curcumin can change the aggregation of proteins as they provide multifaceted interaction forces with the proteins.[13] Earlier reports have acknowledged that targeting fibrillation monomers might be more efficient to prevent protein aggregation than targeting the maturing fibrils. Curcumin is observed to inhibit fibril formation by both globular proteins and intrinsically disordered proteins. Curcumin interferes with oligomer formation by destabilizing the salt bridge (Asp 23-Lys 28) of Aβ. Furthermore, the additional benefit of curcumin is that they cross blood–brain barrier when given via parenteral route.[8,14–16]

Thus, the design and synthesis of new curcumin derivatives by adding their bioisosteres may provide a molecule with unique properties as compared to the original. Structural activity relationship studies showed that phenolic hydroxyl group and α–β unsaturated β-diketone moiety are essential for anti-amyloidogenic activity. Monosubstitutions in methoxy curcumin analogs showed greater inhibitory activity as compared to disubstituted ones. The curcumin derivatives must have two aromatic ends with a seven-carbon linker for their optimum activity. Thus, chemical library may be prepared to fix the aromatic ends and linkers and to modify the α–β unsaturated β-diketone moiety which revealed enhanced stability and greater therapeutic efficacy.[17,18]

In our study, a chemical library is constructed by fragment-based drug design (FBDD) approach and is screened by docking over the Amyloid-β protein. The best binding ligand was selected based on their docking scores and was further screened over β-secretase protein or β site APP cleaving enzyme (BACE1). BACE1 protein inhibitors are in study nowadays to develop an anti-Alzheimer drug. Dual inhibitor of both Amyloid-β and BACE1 protein is also analyzed based on their binding site interactions to both the proteins and is optimized via *de novo* ligand design. The binding affinity of the best conformer generated via *de novo* is also characterized by molecular docking. Finally, the selected lead was screened through Lipinski's Rule of FIVE, *in silico* toxicity testing, and compared with the drugs already in the clinical trial.

2. MATERIALS AND METHODS

2.1. Materials

The chemical library is created using ChemDraw Ultra 12.0. (CambridgeSoft,100 Cambridge Park Drive, Cambridge) and was analyzed using AutoDock Vina (The Scripps Research Institute, La Jolla, California). Cheminformatics tool eLEA3D is used for *de novo* ligand design (https://chemoinfo.ipmc.cnrs.fr/LEA3D/index.html). Drug likeness was evaluated by Molinspiration (https://www.molinspiration.com/cgi-bin/properties) and *in silico* screening for toxicity was carried out using admetSAR 2.0(http://lmmd.ecust.edu.cn/admetsar2/) and quantified structural similarity of the best ligand was obtained with the using ChemMine Tools.[19] MD dynamic simulation was carried out to determine the stability study using GROMACS v2020.1 simulation software package using the CHARMM36 forcefield.[20] Pharmacophore mapping (http://zincpharmer.csb.pitt.edu/pharmer.html) was initiated to generate descriptors and determine the features essential for interactions. Docking results and Pharmacophore search results were correlated together.

2.1.1. *Development of chemical library*

Ligands are prepared by substituting various groups in R1, R2, R3, R4, R5, R6 (1–3 and 16–18 position) in the two aromatic rings as shown in the aromatic keto form of Curcumin (Fig. 1). A, B and C is replaced by various isosteres or heterocyclic moieties like pyrazole, isoxazole and isothiazole that may reduce metal chelation of curcumin and enhance inhibition of β and γ

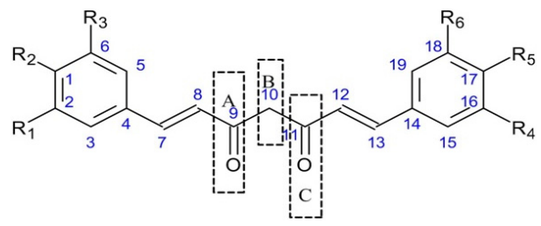

Fig. 1. (Color online) Places of substitutions over curcumin moiety for chemical library design.

secretase.[15,21,22] From the structural activity relationship study, sequential ligand design was carried out by replacing methoxy group with its isosteres in R1or R4 alone and both R1 and R4. The previous study emphasizes replacing A, B, C with various heterocyclic isosteres to acquire unique structural stability, greater binding affinity, and metal chelation effect. Ligands with two group substitutions in both R1 and R4, R2 and R5, R3 and R6 and A, B, C group (C9–C11) and R4 replacement have been assumed to provide best results based on earlier structure-activity relationship studies as mentioned above. The detailed construction of the chemical library has been provided in Table S1.

EQ: Supplementary Table is cited in text. Kindy refer.

2.2. Molecular Docking studies and selection of the lead

The prepared chemical library was docked to evaluate the ligand and amyloid-β (Aβ) protein interaction *via* AutoDock Vina4.2.0.[23] For the Aβ protein, various transition phases of β-pleated protein were downloaded from Protein Data Bank and docked with the designed compounds. *In vitro* amyloid β structures (40–42 amino acids) undergo transitions from soluble protein to the aggregated beta-sheet. These transitions are however considered as our targets and marked as initial, intermediate, and final stages of amyloid β protein structure changes. The initial target protein **(www.rcsb.org, PDB ID: 1IYT)** has two helical regions connected with a flexible 'kink'. The NMR structure of intermediate target protein **(www.rcsb.org, PDB ID: 1Z0Q)** shows that change of external environments from nonpolar to polar environments, leads to loss of C-terminal helix but N-terminal helix is retained. The final stage of target protein **(www.rcsb.org, PDB ID: 2BEG)** contains residues 1–17 which are disordered and residues 18–42 form a beta-strand (residues 18–26), then the residues turn to form a salt bridge (residues 27–30) and a second beta-strand (residues 31–42). Generally, two molecules of Amyloid β (residues 1–42) are required to achieve the protofilament structure.

The ligand was designed to target initial **(www.rcsb.org, PDB ID: 1IYT)**, intermediate **(www.rcsb.org, PDB ID: 1Z0Q)**, and final stage **(www.rcsb.org, PDB ID: 2BEG)** of Amyloid β protein. The alpha helix structures of the given protein decrease from initial protein stage and a considerable increase of beta-sheet is observed in the final stage of Amyloid β **(www.rcsb.org, PDB ID: 2BEG)**. (Figs. S2 and S3)

EQ: Supplementary figures are cited in text. Kindly refer.

Additionally, the selected molecules based on their docking scores exhibited considerable binding interactions with BACE-1 and the ligand-BACE-1 complex inhibits protein fibrillating pathway by attenuating the cleavage of the APP. We assume that the above approach may help in preventing protein fibrillation by destabilizing the protein fibrils themselves in the initial, intermediate and final stages of aggregation.

The ligands were designed by structure-based drug design and listed in the given table (Table S1). Thus, the chemical leads with the best docking scores against the above proteins were selected and redocked with beta-site APP cleaving enzyme or BACE1 enzyme protein **(www.rcsb.org, PDB ID: 2ZHT)**.[24] The binding affinity was evaluated and the binding site was analyzed with both 2BEG and 2ZHT. The classes of forces responsible for ligand-protein interaction were screened in BIOVIA Discovery Studio Visualizer 2020 (Dassault Systèmes, San Diego, USA). *de novo* ligand design using LEA3D was further carried out to ensure lead optimization.

2.3. *de novo* ligand design

de novo ligand design was used for lead modification of the best fitting ligand in docking. The software e-LEA3D has been used for the purpose where protein structure in PDB format was used as input, and the residue details around the binding site together with the .sdf file of the ligand (along with their atom numbers) was provided as further specifications. Ten cycles of the run were allowed which worked on genetic algorithm coupled with ligand-protein docking and the results were generated based on the best binding profile with the input protein and with the threshold fitting scores of 60–70% with the parent ligand.

2.4. Evaluation of Lipinski's rule of five and admetSAR of the selected lead

Lipinski's Rule of Five was evaluated using MOLINSPIRATION server for the selected lead to unfold its *in silico* potential to become a drug. *In silico* toxicity data was generated from admetSAR server.[25] The best lead was selected as the candidate molecule and was analyzed for its similarity index with available drugs for alzheimers in AD or MK-8931(Verubecestat) using ChemMine tools.[26] The structural similarity was searched by both the Tanimoto index and the manual pharmacophore search method.

2.5. Molecular dynamic simulation

All MD simulations were carried out using the GROMACS v2020.1 simulation software package using the

DOI: 10.1142/S2737416522500193
J. Comput. Biophys. Chem. **2022**

CHARMM36 forcefield[27] with Periodic Boundary Conditions. Topology files for the target peptide molecule were made using GROMACS while the same for the ligand was generated using the SwissParam online tool,[28] as per the standard protocol, and the two merged to obtain the topology of the desired complex.

2.5.1. *Root mean square fluctuations (RMSF) plots*

The complex thus obtained was solvated within a dodecahedron simulation box measuring at least 1.0 nm on each side of the peptide and hydrated using the Steepest Descent algorithm. Before MD run, the system consisted of SPC216 water model. The residual charges on the system thus generated were neutralized by replacing the solvent molecules with Na^+ or Cl^- as counter ions and subjected to 50,000 steps energy minimization process-ligand complex, solvent molecules and ions were equilibrated using NVT and NPT ensembles, respectively with a constrained system ($\sim$1000 kJ/mol nm^2) for 100 ps at 300 K. Finally, the position restraints were released and production runs for the desired systems were carried out at 300 K for 2 ns. The output trajectories were recorded every 10 ps for data analysis. Simulation data visualization was done through VMD software package. Minimum peptide-ligand distances and the RMSD of the peptide backbone/ligand during the simulation run were evaluated using GROMCS tools. The peptide-ligand hydrogen bonds formed during the simulation run were monitored using VMD 1.9.3 software package where the maximum donor–acceptor distance was maintained ≤ 0.35 nm and hydrogen-donor–acceptor angles $\leq 30°$. The participation of the amino acids within the peptide secondary structural dynamics over the simulated time period was also calculated using the VMD software.

2.5.2. *Dictionary of secondary structure of protein (DSSP) algorithm plots*

Aβ42 has an N-terminal domain and a flexible C-terminal prion forming domain. The secondary structure of Aβ42 includes the transition of α-helix and β-sheet structures. Our ligand targets the β-sheet of protein, thus protein dynamics are checked at picoseconds and angstrom level resolutions to elucidate the transitions at the molecular level. The secondary structure transition of Aβ-42 was monitored using DSSP, which uses geometric pattern and hydrogen bond recognition for secondary structure determination. Aβ-42 sheet extends from 2–6 residues to align with other β strands.[29,30]

2.6. Pharmacophore mapping

To support our previous study, we correlate our previous finding with ligand-based drug design where we have complete information of our ligand. We shall generate 3D structures of various conformers of ligands and various features responsible for interaction are marked accordingly. The pharmacophore is used for 3D database search queries. The step-in pharmacophore mapping includes conformer generation of molecular structures and low energy conformers are chosen and the features are aligned.[31] The pharmacophore model expressing descriptors such as hydrophobic interaction, hydrogen bonding interaction, ionizable interaction, hydrogen bond donor and acceptor interaction was shown with different regions.[32]

3. RESULTS AND DISCUSSIONS

3.1. Molecular docking studies of compound (49) and curcumin with 1IYT, 1Z0Q, 2BEG and 2ZHT

As per earlier reports, optimal activity of curcumin or curcuminoids requires the phenolic aromatic group and the seven carbon linkers between two terminal aromatic rings along with polyhydroxy groups and ketonic moiety in its structure.[33,34] Modifications by introducing bioisosteres of $-OCH_3$ such as –F, $-CHF_2$, $-CF_3$, $-CF_2CH_3$, $-SCH_3$ and –OH resulted in variations of R1 and R4. Docking scores of such modifications mostly ranged between −5.0–6.2 Kcal/mol. Similarly, modifications in R2, R3, R5 and R6 showed comparatively less binding scores such as −5.3–6.0 kcal/mol. However, substitutions with heterocyclic moiety like pyrazole and its derivatives yielded compounds **47, 31, 27, 26, 38, 44, (49), 30** that revealed docking scores in between −6.4–6.8 Kcal/mol, greater than that of standard curcumin (−5.5 Kcal/mol). Derivative with isoxazole in compounds **45** and **42** showed a considerable docking score with **2BEG** (−7.2 and −6.5 Kcal/mol, respectively). At least, 10 best leads were taken and redocked on BACE1 **(2ZHT)** to reveal greater binding affinity than curcumin, of which the pyrazole ring containing compounds displayed preferentially higher docking scores such as −9.4 **(44)**, −9.3 **(45)**, −8.7 **(49)**, −8.8 **(31)**, −8.9 **(30)**, −8.3 **(26)** Kcal/mol. Oxazole containing analog **(45)** also exhibited considerable binding affinity of −9.4 Kcal/mol (concomitant with **44**) but elicited lesser binding activity with 2ZHT compared to others, thus was not selected as the best lead (detailed docking scores of each compound is not shown here).

AQ: Kindly approve edit.

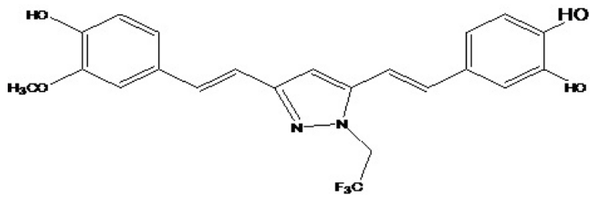

Fig. 2. Compound (**49**) (Best selected lead from 2BEG and 2ZHT Docking scores).

The compound (**49**) (Fig. 2) was selected as the best lead as it showed greater interaction and binding affinity compared to others in the library. Our lead compound exhibited greater binding interaction and enhanced dock score. The force interaction map revealed that dihydroxy moiety present on two aromatic rings of the molecule plays an orchestral role in binding with the protein in compliance with the earlier report that multiple hydroxyl groups aids in potent activity of curcumin by exerting similar kind of interactions with the target protein.

Receptor **(2BEG)** exhibits π–π stacking with Phe19 and reaches the core of fibril or KLVFFAE fragment (Fig. 3(a)). Compound **(49)** also showed a plethora of binding interactions with the target BEG when analyzed in Discovery Studio Visualizer 2020. Notably, Ala 21 showed π–π interaction between the peptidic bond present over it and the aromatic ring bearing –OCH_3 group in the compound (Fig. 3(b)). In addition, Glu 22 exerts van der Waals interaction with the –CH_3 group present over the ring. Most interestingly, Asp 23 is found to establish hydrogen bonding interactions with the highly electronegative –F atoms over –CF_3 bonded with the central pyrazole nucleus. Lys 28 and Gly 29 which are adjacent to the kink forming region of 26–27 amino acid residues, are also revealed to set van der Waals interaction with the compound. Encompassing all these forces of interaction in between the compound **(49)** and the 2BEG, it may be extrapolated that the former may stabilize the latter (Aβ-42 peptide) with considerable binding especially into the core site and folding region, thus inhibiting it to transform into further plaques of amyloid sheets.

Now, the question arises, can compound **(49)** inhibit or stabilize BACE-1 (β-secretase) to exert a dual role in inhibiting β-amyloidogenesis? To elucidate that, we analyzed the binding map with compound **(49)** with PDB isoforms of BACE-1 (2ZHT). The compound showed direct interaction with Ala 157 and Val 170 with hydrogen bonding while both of these amino acids are buried in the active site of the protein as reported in earlier citations where it has been acknowledged that Asp 32 to Asp 228, the entire region act as an active site of the BACE-1 protein.[35] Moreover, Ser 10 and Gly 11

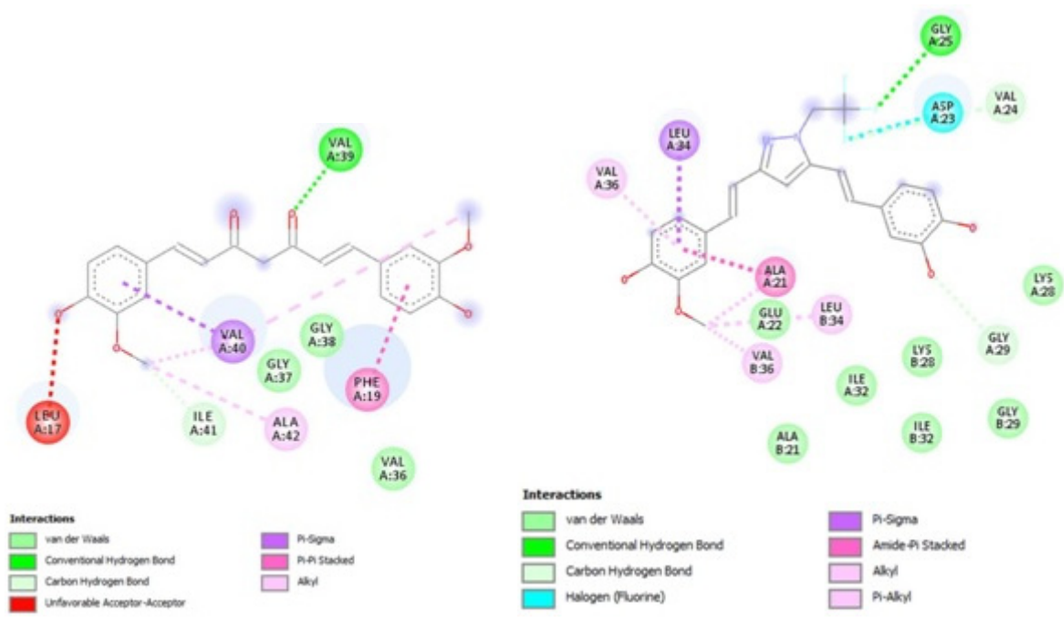

(a) (b)

Fig. 3. (Color online) Comparison of 2BEG binding site interactions. (a) Standard curcumin and (b) Compound **(49)**.

DOI: 10.1142/S2737416522500193
J. Comput. Biophys. Chem. **2022**

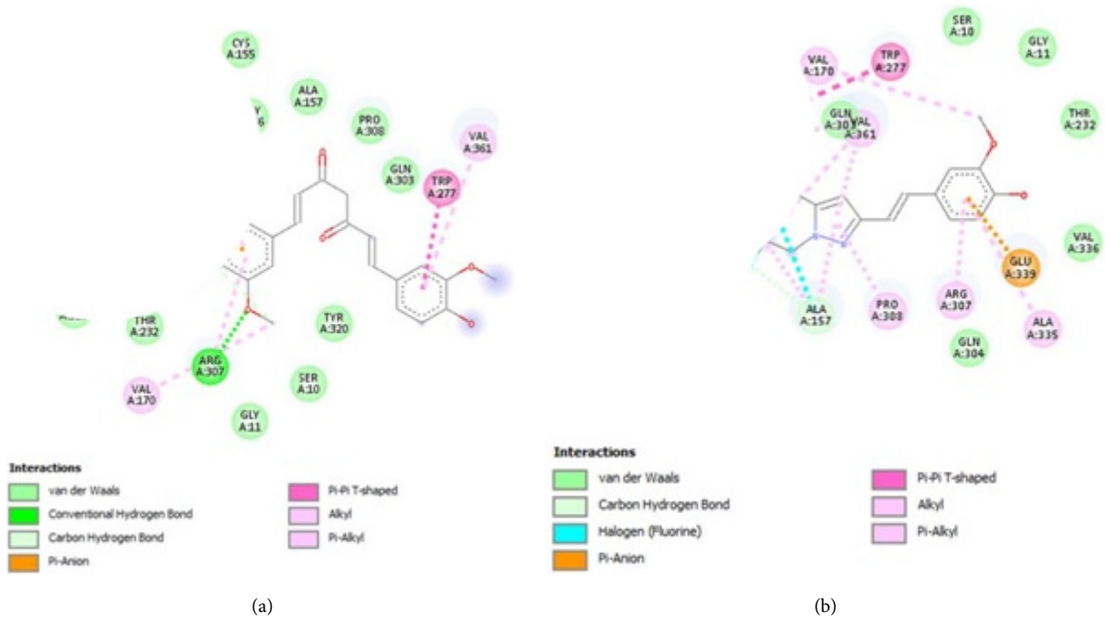

(a) (b)

Fig. 4. (Color online) Comparison of 2ZHT binding sites (a) Standard curcumin and (b) Compound **(49)**.

amino acids lie in S3 binding pocket (loop 10s) which bears a pivotal role in stabilizing the binding of the incoming compound Interestingly in our study, both these amino acids exert van der Waals force of interaction with the compound **(49)** which might play additional role in reinforcing the compound interaction with the binding site (Fig. 4(B)). Interactions of 2BACE1 with standard also showed similar kinds of interactions involving both active site and loop 10s (Fig. 4(A)). Thus, compound **(49)** has not only shown better docking scores than standard curcumin (Table 1) against both 2BEG (−6.8 Kcal/mol and −5.5 Kcal/mol, respectively) and 2ZHT (−8.7 Kcal/mol and −7.9 Kcal/mol, respectively) but also has exhibited binding site penetration comparable with the standard.

Pyrazole replacement **(49)** gives better result showing that the cyclic ring in the symmetric region gives more stability to the structure of Curcumin as they show lower binding energy. The presence of nitrogen shows greater binding efficiency in BACE1.

Table 1. Docking score of Standard and compound (49) with 2BEG & 2ZHT.

Molecule	Docking score (2BEG) (Kcal/mol)	Docking score (2ZHT) (Kcal/mol)
Std (Curcumin)	−5.5	−7.9
Compound (49)	−6.8	−8.7

This compound was docked with another **initial (1IYT)** and **intermediate stages (1Z0Q)** of protein. Furthermore, the pyrazole ring might enhance the stability of the same for target protein binding by possible hydrogen bonding interactions between the two basic nitrogen atoms over the ring (acting as hydrogen bond acceptors) and the polar hydrogen of the protein. The pyrazole ring shows van der Waals interaction with **1IYT (the initial stage of Amyloidβ)** Asp 23, Gln 15, Glu 22 **(Fig. S4).** Similar interactions were achieved with our final target protein (2BEG). Similarly, our lead compound was docked with **intermediate stages (1Z0Q)** and they exhibited strong hydrogen bonding with Glu 35. Other protein interactions like van der Waals interaction were exhibited with Glu 31, π–π stacking was observed with Phe 14, and π–anion bonding with Glu 22 **(Fig. S5).**

EQ: Supplementary figure is cited in text. Kindly refer.

3.2. *De novo* ligand design

De novo ligand design of **(49) with amyloid fibril (2BEG) protein** shows **63.30%–68.00%** scoring function that may be an appropriate choice for selecting *de novo* sequence for further consideration. However, **(49) with BACE1 (2ZHT) protein** shows **53.64%** scoring function. The genetic algorithm of the first generated offspring's of compound ((**49**)) resulted in various scaffolds with an improved fitting score with the parent scaffold. **(49)_scaffold 7 (Fig. S6)** being generated with

EQ: Supplementary figure is cited in text. Kindly refer.

Table 2. Lipinski's Rule of Five evaluation of selected leads.

Parameters in Lipinski's Rule of Five	Compound (49)	Compound 49_scaffold 7
miLogP *	4.92	7.12
MW *	432.40	508.50
nON *	6	6
nOHNH *	3	2
No. of rotatable bonds	7	9

Notes: *miLogP-Molinspiration LogP, MW-Molecular Weight, nON-number of hydrogen bond acceptors, nOHNH-number of hydrogen bond donors

AQ: Kindly provide this symbol inside the table too.

more structural similarity with parent ((**49**)), was chosen on pharmacophore similarity basis; and subsequently was redocked to reveal binding affinity as −6.4 Kcal/mol with **2BEG** and −7.5 Kcal/mol with **2ZHT**. It shall thus enhance chances of success to design another lead with promising anti-amyloidogenic activity together with parent compound **(49)**. This tool is used to find a new ligand that optimizes a user-specified scoring function.

Both compound **(49)** and **scaffold 7** have passed the Lipinski rule of five. The first compound exhibited a milogP value of 4.92 with a molecular weight of 432.40, with 3 and 6 hydrogen bond donors and acceptors, respectively. Although the second compound exhibited a little bit higher log P (7.12) than the permissible value (5.0), the other parameters complied with the permissible parameters of Lipinski's Rule (**Table 2**).

They exhibited drug likeliness and *in silico* toxicity studies showed that they are not carcinogenic or mutagenic and could cross Blood–Brain Barrier (BBB) **(Table 3)** which may be a promising finding to target Alzheimer's disease in the brain. They have also not shown any inhibitory potential towards steroid and thyroid binding receptors as revealed by admetSAR (detailed data not shown here).

Table 3. *In silico* toxicity evaluation by admetSAR.

Parameter	Curcumin	Compound (49)	Compound (49)_scaffold 7
BBB	−	+	+
CYP 2C9 inhibition	+	+	+
CYP 3A4 inhibition	−	−	−
Hepatotoxicity	+	−	−
Carcinogenicity	−	−	−
Mutagenicity	−	−	−
p-glycoprotein inhibition	+	−	−

Note: +means toxicity found, −means no toxicity found.

3.3. Comparative study of our leads with Verubecestat

Finally, the compound **(49)** is compared to get the similarity index with the results of marketed MK-8931 (Verubecestat) and compound **(49)**.[36] The compound showed slight similarity with MK-8931(Verubecestat) having AP Tanimoto of 0.194051 (Fig. S7). Verubecestat has aromatic groups namely pyridine and thiadiazole and compound **(49)** has 1-hydroxy-2-methoxyphenyl aromatic groups in the terminal end. The central pyrazole ring is separated by two carbon from phenolic ends in compound **(49)** which is close to the structure of Verubecestat having two-atom separations in between fluorophenyl and pyridine. Thus, compound **(49)** has slight but existing structural resemblance with MK-8931(Verubecestat).

3.4. Molecular dynamic (MD) simulation study

3.4.1. *Root mean square fluctuations (RMSF) plots*

The peptide and ligand were found to achieve stable conformations within the first 200 ps of the simulation run, beyond which we did not find any significant shift within their respective RMSDs. The minimum peptide–ligand distance during the entire simulation run was found to be 0.205 ± 0.018 nm, indicating stable interaction between the two moieties under consideration. This is further substantiated by the observed 1.336 mean peptide–ligand H-bonds over the entire simulation run where the two molecules under consideration were found to be H-bonded for approximately 80% of the entire period, particularly with the Ala 21 of the A-beta peptide. All these observations indicated that our docked ligand can interact well with our target peptide. (Fig. 5)

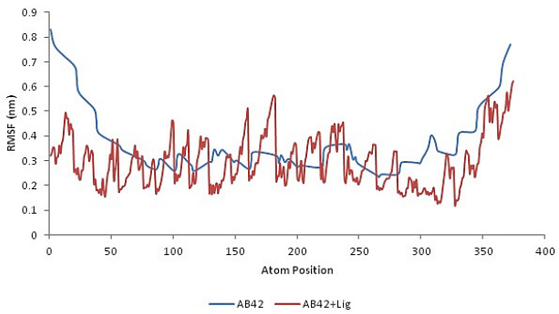

Fig. 5. (Color online) RMSF plot of compound **(49)** alone and Aβ-42 and compound **(49)**.

DOI: 10.1142/S2737416522500193
J. Comput. Biophys. Chem. **2022**

3.4.2. *Dictionary of secondary structure of protein (DSSP) algorithm plots*

The secondary structure transitions of the Aβ protein and Aβ protein along with the ligand (compound 49) were observed by DSSP plots. The DSSP plots provide an image with some color scale key, as indicated in Fig. 6. The color scale keys are labeled as "sec. struct." and are remarked with letter such as T, E, B, H, G, I, C of which T refers to 'Turn', E stands for 'extended configuration', B mentions the presence of 'isolated bridge' or loop. The color scale key E indicates the main conformation of β-sheet, T or aqua is another component of β-sheet and B also refers to the isolated bridge. The H stands for alpha helix region, G refers to another secondary structure, 3–10 helix, I indicates π helix and C stands for a random coil. The color bands indicate secondary structure determination with respective residues change concerning nanosecond time frame.[29]

The transition of the secondary structure of Aβ with and without ligand is verified and the disruption of the β-dimer formation and β-sheets of each monomer were also observed. The DSSP plot of Aβ protein elucidates that the N-terminal α-chain remains retained but C-terminal gets converted to β-sheets, β-turns and loops. The standard secondary structure of protein is defined by the residues spending more than 50% of simulation time in α-helix or β-sheet at a standard temperature (25°C). **Leu 17 & Val 18** show random

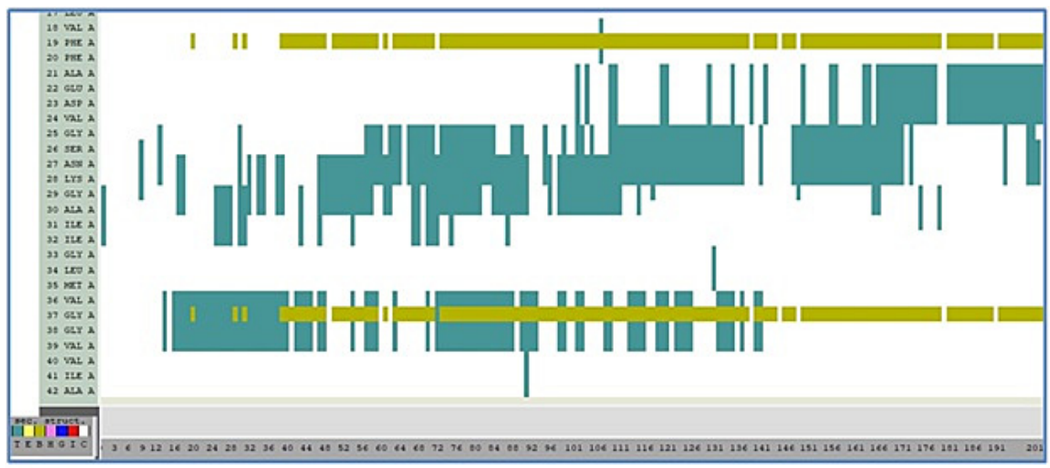

(a)

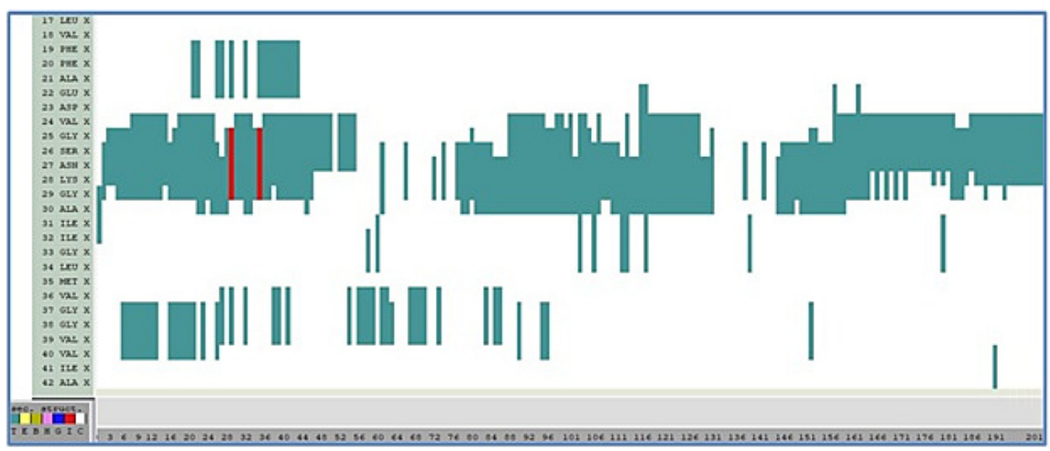

(b)

Fig. 6. (Color online) DSSP plot for secondary structure transition of protein (a) 2BEG (Aβ alone) and (b) 2BEG (Aβ + compound **(49)**).
***Secondary Structure codes represent T-(β turn), E-Extended β configuration, B-Isolated loop, H-αhelix, G-3-10 helix, I-5 helix, C-Coil.**

AQ: Kindly clarify if this belongs to any footnotes and if it is kindly provide symbol for it.

coiling throughout the 200 ns time scale (Fig. 6(a)). Single pair β sheet hydrogen bond or isolated bridge region was highlighted with a different color in two regions namely, **Phe 19 & Gly 37.** Consistent β turns are observed in residues **Ala 21-Val 24 and Val 36-Val 39. Gly 25-Ala 30** undergoes β transitions from the coil to β-turns however β turns remain for a longer time. Residue **Ile 31 & 32** exhibited disarranged behavior throughout the 200 ns time scale. No coil regions are **Gly 33, Leu 34** and **Met 35**.

Thus DSSP plots of the ligand along with protein were studied in the same time frame as above as in Fig. 6(b). The time frames when the β strand begins to completely lose its secondary structure are identified. Partial conversion of β turn to random coil was recorded after 40 ns for residues **Phe 19-Glu 22**. The initiator region in salt bridge or **Asp 23** also exhibits no β-turn region. Compared to other regions of the peptide, the salt bridge region or residues **Val 24-Gly 29** appear to have a higher β sheet forming propensity and existed as β-turns (T region). However, these residues got disordered in 60–80 ns, thus indicating their decreased stability. The C-terminal residues **Ile31-Leu 34** exhibited less β-turns oriented surface. In the first 20 s, **Gly 37-Val 40** recorded β-turn but no such turns were recorded after the given time frame. Mostly, other residues recorded decreased β-sheet regions or random coiling regions. The ligand, compound **(49)** targets the core for fibril formation thus the secondary structure of protein show lesser propensity of β-sheet. Oligomers tend to form large aggregates in the salt bridge region and in the C-terminal region. The regions of isolated bridge are not observed along with the ligand as the functional groups of our ligand change the aggregation of proteins. The ligand forms multifaceted interaction forces with the Aβ protein. The regions of fibril core formation are Lys 16-Glu 22. About the secondary structural dynamics of the peptide, the majority of the peptide residues retain a random coil conformation with few patches of the peptide engaged in retaining the 'Turns' of the peptide. However, the ligand-bound and unbound state of the molecule can be distinctly differentiated by the participation of the 19-Phe and 37-Gly residues in forming isolated bridge conformation for the majority of the simulation time.

3.5. Pharmacophore mapping

A pharmacophore description includes 3D representation of various functional groups and their geometric pattern. These helps in identifying the binding regions responsible for biological activity and active compound conformations are generated to determine the 3D relationship for each conformer.[37,38]

Pharmacophoric features correlate physical, chemical, and structural attributes to the biological activity of the molecule. Thus, pharmacophore features of our lead compound display descriptors like three aromatic regions, two hydrogen bond donors, five hydrogen bond acceptor regions and various hydrophobic regions as in Fig. 7. The features are identified by ligand alignment and the active features required for receptor binding is identified to correlate the findings obtained from docking.

After developing the pharmacophore features, the combination of descriptors essential for binding was studied closely. Docking results vividly emphasize on hydrogen bonding interactions with Asp 23 of 2BEG

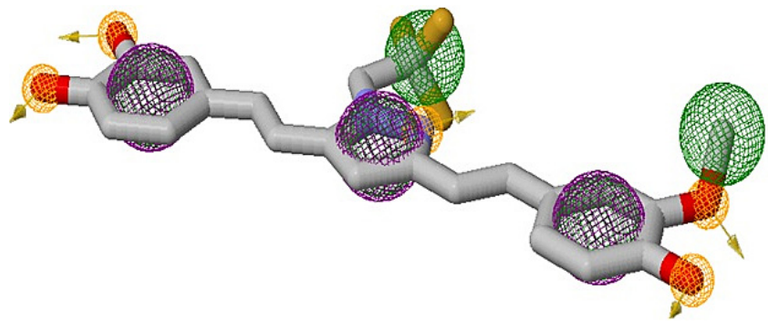

(a)

Fig. 7. (Color online) (a) harmacophore modeling of compound **(49)** exhibiting various descriptors signifying, aromatic (purple), five hydrogen acceptor regions (orange), two hydrogen donor regions (green). (b) Pharmacophore descriptor alignment from Zinc Pharmar.

DOI: 10.1142/S2737416522500193
J. Comput. Biophys. Chem. **2022**

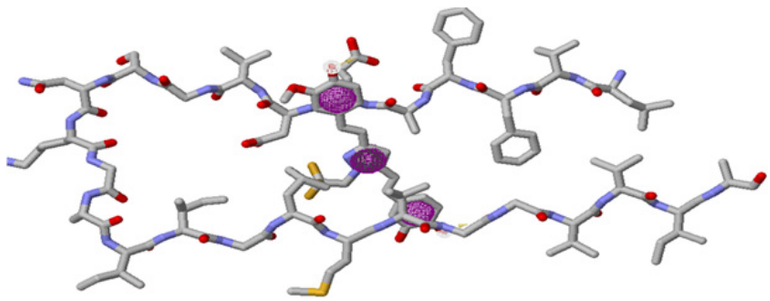

(b)

Fig. 7. (*Continued*)

protein. Pharmacophore results also clearly explain the hydrogen bond acceptor regions of Asp 23 binds to hydrogen donor regions of $-CF_3$. Similarly, van der Waals interaction is observed in docking as well as pharmacophore search results of Glu 22 and Lys 28 with hydrogen donor regions of $-CH_3$ group. Ala 21 has no hydrogen bond donor or acceptor regions thus exhibiting $\pi-\pi$ interaction with the aromatic descriptors of compound 49.

3D pharmacophore search results can generate similar active molecules in the zinc database. Such database manifests the generation of various possible pharmacophores with their RMSD values or deviation values from the original lead compound along with their structure **(Table S3)**. The generated active molecules are coded with names as initial 'ZINC' signifying the zinc databases of active molecules. Zinc database tabulated similar five molecules with active regions and similar geometric pattern. Thus, Lead compound **(49)** can be elucidated as an active molecule with set of features that is common to some series of active molecules.

4. CONCLUSION

Our drug designing through scaffold hopping over Curcumin has led a generation of a promising lead, compound **(49)** with a centrally placed pyrazole nucleus flanked with two or three aromatic rings together with three central fluorine atoms. Curcumin substituted with pyrazole replacing the diketone moiety may provide extra stability to the curcumin structure, improve amyloid β protein binding site interactions and enhance its BBB permeability. Heterocyclic group insertion by replacing the α-β unsaturated β-diketone showed higher docking scores as compared to standard thus proving that cyclization of the ketone groups using various isosteres can develop more potential leads against β-amyloidogenesis. Dual inhibitors were designed and the β-secretase was targeted along with amyloid-β protein through our rational drug design (RDD). Pyrazole and substituted pyrazoles such as 1-chlorophenylpyrazole, 1-bromophenylpyrazole, 1-methylphenylpyrazole, 1-methoxy pyrazole, 1-difluoromethylpyrazole showed promising results along with isooxazoles derivative of curcumin in our RDD. Information of the target protein enabled us to design a molecule based on structure-based drug design which was comprised of designing a chemical library and then docking them against various transition phases of protein **(1IYT, 1Z0Q, 2BEG)** and BACE-1 protein **(2ZHT)**. Best docked compound was selected and was compared to available marketed lead after de novo ligand based drug design. Amongst them, Compound 49 having 1-difluoromethylpyrazole exhibited good *in silico* docking results and may be regarded as a promising lead for developing as dual inhibitors.

The *in silico* drug design study was adopted to design novel leads against Alzheimer's disease. A chemical library was designed based on various literature surveys and the leads were screened based on their docking score. The best ligand with appropriate drug likeliness and no toxicity was selected to be docked for various other stages of amyloid beta fibrillation (initial, intermediate, final stages) and further were docked against BACE-1 peptide. This lead was referred to as a dual inhibitor and *de novo* ligand-based study was carried out to obtain other conformers of our lead. However, this did not give relevant results. Next, the molecular dynamic simulation was carried out to predict the stability of the molecule while the protein undergoes a transition of α and β sheets. RMSD plots of Aβ alone and Aβ+compound were verified to undergo the transitions of protein in nanosecond time

frame with and without the ligand. The selected lead remains stable in all such transition phases of protein. DSSP plots also exhibited that the winner molecule hindered α-helix to β-sheet transition for many residues in the binding pocket which is also the seeding zone of β–β dimerization. Additional docking of the chosen winner, compound **(49)** with BACE-1 enzyme also revealed that the ligand can occupy the core binding pocket and engages the critical amino acid residues such as Asp 32, Asp 228, Gly 11 (loop 10s). Hence, it may be deciphered that compound **(49)** may have dual inhibitory role both on Aβ-42 and BACE-1. Lastly, major contributory segments were found by ligand-based drug design or pharmacophore mapping for further investigations.

Thus, compound **(49)** may be considered as promising dual active leads for treating Alzheimer's disease or related protein fibrillation disorders (β-amyloidogenesis) and can be subjected to further investigations for future studies.

ACKNOWLEDGMENT

The authors are thankful to Dr. B. C. Roy College of Pharmacy & Allied Health Sciences, Durgapur, WB, India for providing all the support for executing this work.

References

1. Ahmad, B.; Borana, M. S.; Chaudhary, A. P. Understanding Curcumin-induced Modulation of Protein Aggregation. *Int. J. Biol. Macromol.* **2017**, *100*, 89–96, https://doi.org/10.1016/j.ijbiomac.2016.06.053.
2. Narlawar, R.; Baumann, K.; Schubenel, R.; Schmidt, B. Curcumin Derivatives Inhibit or Modulate Beta-Amyloid Precursor Protein Metabolism. *Neurodegener. Dis.* **2007**, *4*, 88–93, https://doi.org/10.1159/000101832.
3. Chan, S. *et al.*, Metal Chelation, Radical Scavenging and Inhibition of Aβ42 Fibrillation by Food Constituents in Relation to Alzheimer's Disease. *Food Chem.* **2016**, *199*, 14–24, https://doi.org/10.1016/j.foodchem.2015.11.118.
4. Zhang, C.; Browne, A.; Divito, J. R.; Stevenson, J. A.; Romano, D. Amyloid-β Production Via Cleavage of Amyloid-β Protein Precursor is Modulated by Cell Density. **2010**, *22*, 683–694, https://doi.org/10.3233/JAD-2010-100816.
5. Strooper, B De. Amyloid-Beta Precursor Protein Processing in Neurodegeneration. **2004**, 582–588, https://doi.org/10.1016/j.conb.2004.08.001.
6. Scheuermann, S. *et al.*, Homodimerization of Amyloid Precursor Protein and Its Implication in the Amyloidogenic Pathway of Alzheimer's Disease. **2001**, *276*, 33923–33929, https://doi.org/10.1074/jbc.M105410200.
7. Ramshini, H.; Mohammad-Zadeh, M.; Ebrahim-Habibi, A. Inhibition of Amyloid Fibril Formation and Cytotoxicity by a Chemical Analog of Curcumin as a Stable Inhibitor. *Int. J. Biol. Macromol.* **2015**, *78*, 396–404, https://doi.org/10.1016/j.ijbiomac.2015.04.038.
8. Cui, L. *et al.*, Effect of Curcumin Derivatives on Hen Egg White Lysozyme Amyloid Fibrillation and their Interaction Study by Spectroscopic Methods. *Spectrochim Acta - Part A Mol Biomol Spectrosc* **2019**, *223*, 117365, https://doi.org/10.1016/j.saa.2019.117365.
9. Palumbo Piccionello, A. *et al.*, Synthesis and Preliminary Antibacterial Evaluation of Linezolid-like 1,2,4-Oxadiazole Derivatives. *Eur. J. Med. Chem.* **2012**, *50*, 441–448, https://doi.org/10.1016/j.ejmech.2012.02.002.
10. Liu, G.-Y., Amro, N. A. Positioning Protein Molecules on Surfaces: A Nanoengineering Approach to Supramolecular Chemistry. *Proc. Natl. Acad. Sci.* **2002**, *99*, 5165–5170, https://doi.org/10.1073/pnas.072695699.
11. Curcumin, N., Ahsan, N., Mishra, S., Jain, M. K., Surolia, A., Gupta, S. Modulate Toxicity of Wild Type and 2015, https://doi.org/10.1038/srep09862.
12. Chen, G. F. *et al.*, Amyloid Beta: Structure, Biology and Structure-based Therapeutic Development. *Acta Pharmacol. Sin.* **2017**, *38*, 1205–1235, https://doi.org/10.1038/aps.2017.28.
13. Nurfina, A. N., Reksohadiprodjo, M. S., Timmerman, H., Jenie, U. A., Sugiyanto, D., Van Der Goot, H. Synthesis of some Symmetrical Curcumin Derivatives and their Antiinflammatory Activity. *Eur. J. Med. Chem.* **1997**, *32*, 321–328, https://doi.org/10.1016/S0223-5234(97)89084-8.
14. Konno, H. *et al.*, Synthesis and Evaluation of Curcumin Derivatives toward an Inhibitor of Beta-site Amyloid Precursor Protein Cleaving Enzyme 1. *Bioorganic Med. Chem. Lett.* **2014**, *24*, 685–690, https://doi.org/10.1016/j.bmcl.2013.11.039.
15. Narlawar, R. *et al.*, Curcumin-Derived Pyrazoles and Isoxazoles: Swiss Army Knives or Blunt Tools for Alzheimer's Disease? *Chem. Med. Chem.* **2008**, *3*, 165–172, https://doi.org/10.1002/cmdc.200700218.
16. Fang, L.; Gou, S.; Liu, X.; Cao, F.; Cheng, L. Bioorganic & Medicinal Chemistry Letters Design, Synthesis and Anti-Alzheimer Properties of Dimethylaminomethyl-substituted Curcumin Derivatives. *Bioorg. Med. Chem. Lett.* **2014**, *24*, 40–43, https://doi.org/10.1016/j.bmcl.2013.12.011.
17. Endo, H.; Nikaido, Y.; Nakadate, M.; Ise, S.; Konno, H. Bioorganic & Medicinal Chemistry Letters Structure Activity Relationship Study of Curcumin Analogues toward the Amyloid-Beta Aggregation Inhibitor. *Bioorg. Med. Chem. Lett.* **2014**, *24*, 5621–5626, https://doi.org/10.1016/j.bmcl.2014.10.076.
18. Broe, G. A. *et al.*, Anti-Inflammatory Drugs Protect against Alzheimer Disease at Low Doses. *Arch. Neurol.* **2000**, *57*, 1586–1591, https://doi.org/10.1001/archneur.57.11.1586.

AQ: Kindly provide complete details for Refs. 11, 22, 25

AQ: Kindly provide abbreviated journal title for Refs. 4-6.

AQ: Kindly provide vol no for Ref. 5.

19. Backman, T. W. H.; Cao, Y.; Girke, T. ChemMine Tools: An Online Service for Analyzing and Clustering Small Molecules. *Nucleic Acids Res.* **2011**, *39*, 486–491, https://doi.org/10.1093/nar/gkr320.
20. Van Der Spoel, D.; Lindahl, E.; Hess, B.; Groenhof, G.; Mark, A. E.; Berendsen, H. J. C. GROMACS: Fast, Flexible, and Free. *J. Comput. Chem.* **2005**, *26*, 1701–1718, https://doi.org/10.1002/jcc.20291.
21. Liu, Y.; Dargusch, R.; Maher, P.; Schubert, D. A Broadly Neuroprotective Derivative of Curcumin. *J. Neurochem.* **2008**, *105*, 1336–1345, https://doi.org/10.1111/j.1471-4159.2008.05236.x.
22. Accepted Manuscript n.d. https://doi.org/10.1002/cbdv.201800366.
23. Allouche, A. Software News and Updates Gabedit — A Graphical User Interface for Computational Chemistry Softwares. *J. Comput. Chem.* **2012**, *32*, 174–182, https://doi.org/10.1002/jcc.
24. Han, X.; He, G. Toward a Rational Design to Regulate β-Amyloid Fibrillation for Alzheimer's Disease Treatment. *ACS Chem. Neurosci.* **2018**, *9*, 198–210, https://doi.org/10.1021/acschemneuro.7b00477.
25. Cheng, F. *et al.*, admetSAR: A Comprehensive Source and Free Tool for Assessment of Chemical ADMET Properties 2012, https://doi.org/10.1021/ci300367a.
26. Kennedy, M. E. *et al.*, The BACE1 Inhibitor Verubecestat (MK-8931) reduces CNS b-amyloid in Animal Models and in Alzheimer's Disease Patients. **2016**, 1–14.
27. Lindahl, E.; Bjelkmar, P.; Larsson, P.; Cuendet, M. A.; Hess, B. Implementation of the Charmm Force Field in GROMACS: Analysis of Protein Stability Effects from Correction Maps, Virtual Interaction Sites, and Water Models. *J. Chem. Theory Comput.* **2010**, *6*, 459–466, https://doi.org/10.1021/ct900549r.
28. Zoete, V.; Cuendet, M. A.; Grosdidier, A.; Michielin, O. SwissParam: A Fast Force Field Generation Tool for Small Organic Molecules. *J. Comput. Chem.* **2011**, *32*, 2359–2368, https://doi.org/10.1002/jcc.21816.
29. Porto, W. F.; Maria-neto, S.; Nolasco, D. O.; Franco, O. L. Screening and Functional Prediction of Conserved Hypothetical Proteins from Proteomics & Bioinformatics Screening and Functional Prediction of Conserved Hypothetical Proteins from Escherichia Coli. *J. Proteom. Bioinform.* **2014**, *7*, 203–213, https://doi.org/10.4172/jpb.1000321.
30. Olubiyi, O. O.; Strodel, B. Structures of the Amyloid β-Peptides A β1-40 and A β1-42 as Influenced by pH and a D-Peptide. **2012**, https://doi.org/10.1021/jp2076337.
31. Ahmad, K.; Balaramnavar, V. M.; Chaturvedi, N.; Khan, S. Targeting Caspase 8: Using Structural and Ligand-Based Approaches to Identify Potential Leads for the Treatment of Multi-Neurodegenerative Diseases. *Molecules* **2019**, *24*, 1827, https://doi.org/10.3390/molecules24091287.
32. Hernández-Rodríguez, M. *et al.*, Design of Multi-Target Compounds as AChE, BACE1, and Amyloid-β1-42 Oligomerization Inhibitors: *In Silico* and *In Vitro* Studies. *J. Alzheimer's Dis.* **2014**, *41*, 1073–1085, https://doi.org/10.3233/JAD-140471.
33. Taylor, P.; Kumar, A.; Srivastava, S.; Tripathi, S.; Singh, S. K. Molecular Insight into Amyloid Oligomer Destabilizing Mechanism of Flavonoid Derivative 2-(4′benzyloxyphenyl)-3-Hydroxy-Chromen-4-one through Docking and Molecular Dynamics Simulations. *J. Biomol. Struct. Dyn.* **2015**, https://doi.org/10.1080/07391102.2015. 1074943.
34. Online, V. A.; Rabiee, A.; Ebrahim-habibi, A.; Ghasemi, A. Nemat-Gorgani M. Food & Function Amyloid Fibrillation in Insulin. **2013**, https://doi.org/10.1039/c3fo00019b.
35. Patel, S.; Vuillard, L.; Cleasby, A.; Murray, C. W.; Yon, J. Technology A. Apo and Inhibitor Complex Structures of BACE (b-secretase). **2004**, 407–416, https://doi.org/10.1016/j.jmb.2004.08.018.
36. Scott, J. D. *et al.* Discovery of the 3-Imino-1,2,4-thiadiazinane 1,1-Dioxide Derivative Verubecestat (MK-8931)-A β-Site Amyloid Precursor Protein Cleaving Enzyme 1 Inhibitor for the Treatment of Alzheimer's Disease. *J. Med. Chem.* **2016**, *59*, 10435–10450, https://doi.org/10.1021/acs.jmedchem.6b00307.
37. Giri, R. K.; Rajagopal, V.; Kalra, V. K. Curcumin, the Active Constituent of Turmeric, inhibits Amyloid Peptide-Induced Cytochemokine Gene Expression and CCR5-Mediated Chemotaxis of THP-1 Monocytes by Modulating Early Growth Response-1 Transcription Factor. *J. Neurochem.* **2004**, *91*, 1199–1210, https://doi.org/10.1111/j.1471-4159.2004.02800.x.
38. Bandyopadhyay, S.; Huang, X.; Lahiri, D. K.; Rogers, J. T. Novel Drug Targets based on Metallobiology of Alzheimer's Disease. *Expert Opin. Ther. Targets* **2010**, *14*, 1177–1197, https://doi.org/10.1517/14728222.2010.525352.

AQ: Kindly provide abbreviated journal title, vol no and page range for Refs. 30, 34.

AQ: Kindly provide vol no and page range for Ref. 33.

AQ: Kindly provide abbreviated journal title and vol no for Refs. 26, 35.